3′-Deoxyribopyranose (4′ → 2′)-Oligonucleotide Duplexes (= *p*-DNA Duplexes) as Substitutes of RNA Hairpin Structures

by **Damian Ackermann**, **Xiaolin Wu**, and **Stefan Pitsch***

Laboratoire de Chimie des Acides Nucléiques, Institut de Chimie Moléculaire et Biologique, École Polytechnique Fédérale de Lausanne, EPFL-BCH, CH-1015 Lausanne (e-mail: stefan.pitsch@epfl.ch)

By automated synthesis, we prepared hybrid oligonucleotides consisting of covalently linked RNA and *p*-DNA sequences (*p*-DNA = 3′-deoxyribopyranose (4′ → 2′)-oligonucleotides) (see *Table 1*). The pairing properties of corresponding hybrid duplexes, formed from fully complementary single strands were investigated. An uninterrupted π-π-stacking at the *p*-DNA/RNA interface and cooperative pairing between the two systems was achieved by connecting them *via* a 4′-*p*-DNA-2′ → 5′-RNA-3′ and 5′-RNA-2′ → 4′-*p*-DNA-2′ phosphodiester linkage, respectively (see *Fig. 4*). The RNA 2′-phosphoramidites **9**–**12**, required for the formation of the RNA-2′ → 4′-*p*-DNA phosphodiester linkage were synthesized from the corresponding, 3′-*O*-tom-protected ribonucleosides (tom = [(triisopropylsilyl)oxy]methyl; *Scheme 1*). Analogues of the flavin mononucleotide (= FMN) binding aptamer **22** and the hammerhead ribozyme **25** were prepared. Each of these analogues consisted of two *p*-DNA/RNA hybrid single strands with complementary *p*-DNA sequences, designed to substitute stem/loop and stem motifs within the parent compounds. By comparative binding and cleavage studies, it was found that mixing of the two complementary *p*-DNA/RNA hybrid sequences resulted in the formation of the fully functional analogues **23**·**24** and **27**·**28** of the FMN-binding aptamer and of the hammerhead ribozyme, respectively.

1. Introduction. – We are aiming to develop new strategies for combinatorial preparation of (potentially) functional RNA structures, such as ribozymes and aptamers[1]), that contain not only the four canonical ribonucleosides, but also sugar- and/or nucleobase-modified analogues. In this context, we have already developed prefunctionalized ribonucleoside building blocks that allow postsynthetic modification of oligoribonucleotides on solid phase [3–5]. The classical approach of finding new aptamers (and eventually ribozymes) involves selection of active compounds from a large, random pool of oligonucleotides and their subsequent enzyme-mediated replication [6]. This approach is very powerful, but restricts the number and type of modifications that can be introduced and evaluated for a given purpose[2]).

In general, functional oligoribonucleotides consist of only one oligonucleotide strand that is responsible for formation of the functional part, usually one or more 'bulbs' (= non-*Watson-Crick*-paired regions on a secondary-structure level), and a

---

[1]) The term 'ribozyme' is used for catalytically active oligo(ribo)nucleotide motifs; initially, such sequences were discovered in simple organisms [1]. 'Aptamers' are oligoribonucleotide motifs that specifically bind other molecules [2].

[2]) There are examples of modified ribozymes that are catalytically more active than their unmodified analogues [7].

structural part, formed by hairpin and/or stem motifs (*Fig. 1*). The purpose of the latter is to bring and hold together the functional entities interacting with the substrate.

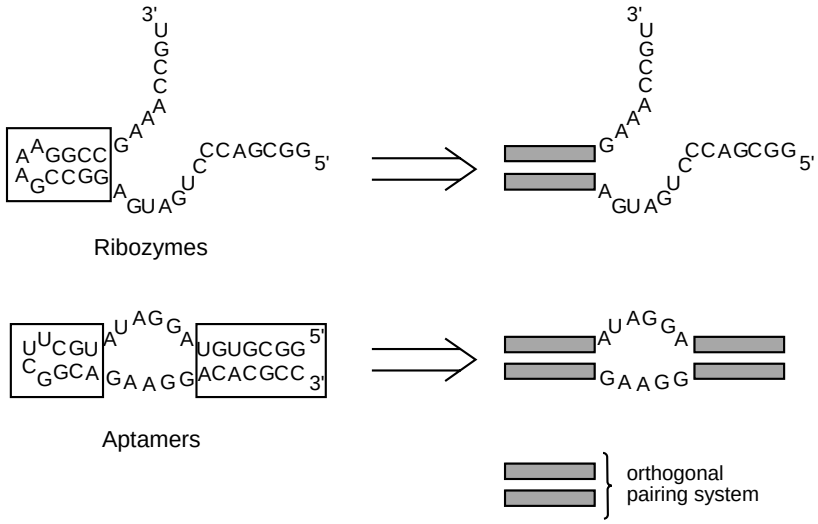

Fig. 1. *Representation of the secondary structures of a hammerhead ribozyme* [8] *and the flavin mononucleotide binding aptamer* [9], *chosen as examples of functional oligoribonucleotide sequences* (left side). *Replacement of the stem loop and stem structures* (shown in boxes) *of such RNA sequences by complementary* p-*DNA sequences* (schematically represented as bars), *thus forming functional oligoribonucleotide motifs by self-assembly of* p-*DNA/RNA hybrid single strands* (right side).

To facilitate the chemical synthesis of a large variety of different potentially functional RNA and related oligonucleotide structures, we wanted to form them from two or more single strands in solution, and substitute the common structural stem loop and stem motifs by complementary duplex structures (*Fig. 1*). In order to avoid any interaction between the functional part of the molecules (consisting of RNA or DNA) and these hairpin-substituting duplex structures, the latter are preferentially formed from an unnatural, autonomous pairing system that pair only with itself, but not with RNA (or DNA).

The autonomous ribopyranose (4′→2′)-oligonucleotide (= *p*-RNA) pairing system, found and investigated by *Eschenmoser* and co-workers [10][11], is one of the strongest and most selective ones, and was, in principle, ideal for our purpose. However, since the synthesis of *p*-RNA oligonucleotides is not compatible with RNA synthesis, we prepared and evaluated 3′-*O*-methyl-ribopyranose (4′→2′)-oligonucleotides (= 3′-*O*-Me-*p*-RNA) and 3′-deoxyribopyranose (4′→2′)-oligonucleotides (= *p*-DNA) as *p*-RNA analogues [12]. Among these three related ribopyranose-based pairing systems, *p*-RNA clearly forms the strongest duplexes, followed by *p*-DNA and 3′-*O*-Me-*p*-RNA. In the above-mentioned context, we finally chose *p*-DNA as autonomous pairing system and subsequently improved its pairing properties by substitution of the nucleobases adenine and cytosine with the analogues purine-2,6-diamine (D) and 5-methylcytosine (M), respectively (*Fig. 2*) [12].

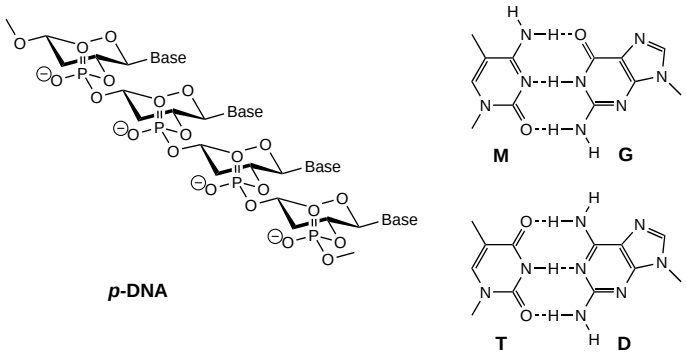

Fig. 2. *Structure and idealized conformation of the* p-*DNA backbone and of the* Watson-Crick *base pairs formed between the nucleobases 5-methylcytosine* (M) *and guanine* (G), *and between thymine* (T) *and purine-2,6-diamine* (D)

This work describes the preparation of *p*-DNA/RNA hybrid sequences, their pairing properties, and the results of our initial studies with *p*-DNA/RNA hybrid duplexes as analogues of the flavin mononucleotide (= FMN) binding aptamer and the hammerhead ribozyme.

2. Results. – 2.1. *Synthesis of RNA*/p-*DNA Hybrid Sequences.* The *p*-DNA, RNA, and *p*-DNA/RNA hybrid sequences prepared in the context of this study, and the structures of the phosphoramidite building blocks employed for their assembly are presented in *Table 1* and *Scheme 1*, respectively. We already have published the synthesis of the *p*-DNA phosphoramidites **1**–**4** [12] and the 2′-*O*-tom-protected RNA phosphoramidites **5**–**8** (tom = [(triisopropylsilyl)oxy]methyl) [13][14]; the preparation of the 3′-*O*-tom-protected RNA phosphoramidites **9**–**12** from the corresponding 3′-*O*-tom-protected ribonucleosides [14] was carried out according to our standard procedure, with 2-cyanoethyl diisopropylphosphoramidochloridite/$^{i}Pr_2NEt$ in CH_2Cl_2 (*Scheme 1*, *Exper. Part*).

The assembly of *p*-DNA/RNA hybrid sequences on a DNA synthesizer was carried out on a 1-μmol scale and under conditions almost identical to those used for the automated assembly of RNA sequences from 2′-*O*-tom-potected RNA phosphoramidites [14], varying only the coupling time (5 min for *p*-DNA phosphoramidites and 2.5 min for 2′-*O*-tom-protected RNA phosphoramidites) and the acylating agent used in the capping reaction ($(MeOCH_2CO)_2O$ instead of Ac_2O)[3]). According to the trityl assay, the individual coupling yields were $<98\%$ for *p*-DNA phosphoramidites and $>99\%$ for tom-protected RNA phosphoramidites. The deprotection of the *p*-DNA/RNA hybrid sequences was carried out under our preferred conditions, first with 10M $MeNH_2$ in H_2O/EtOH 1:1 for 3 h at 25°, followed by 1M $Bu_4NF \cdot 3H_2O$ in THF/1-methylpyrrolidin-2-one 1:1 for 14 h at 25° [14].

In *Fig. 3*, the anion-exchange HPLC traces of two crude product mixtures, obtained from the assembly of the *p*-DNA/RNA hybrid sequences **27** and **28**, are presented.

---

[3]) To avoid the acetylation of purine-2,6-diamine nucleotides; see [12].

Scheme 1. *Phosphoramidite Building Blocks Employed for the Synthesis of* p-*DNA* [12], *RNA* [14], *and* p-*DNA/RNA Hybrid Sequences*

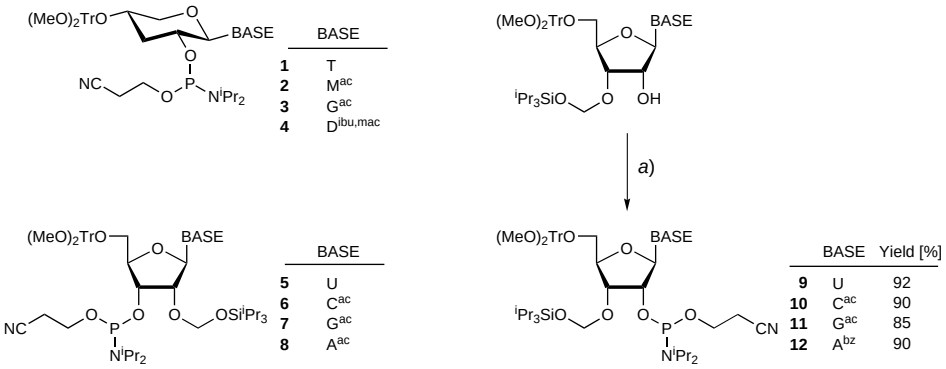

ac = acetyl, ibu = isobutyryl, mac = methoxyacetyl, bz = benzoyl

a) 2-Cyanoethyl diisopropylphosphoramidochloridite, $^{i}Pr_2NEt$, CH_2Cl_2, 25° (see *Exper. Part*)

Table 1. *Preparation and Characterization of RNA*, p-*DNA, and* p-*DNA/RNA Hybrid Sequences*

	Backbone[a])	Oligonucleotide sequence[a])[b])	Isolated yield[c])	MS[d]) [*m*/*z*]	
			a.u. (260 nm)[e])	calc.[f])	found
13	5′-RNA-3′	ACGACGUACU[g])	40	3144.0	3144.3
14	5′-RNA-3′	AGUACGUCGU[g])	38	3161.0	3160.2
15	5′-RNA-3′ → 4′-*p*-DNA-2′	ACGACGUACUDMDMDM[h])	42	5038.3	5038.1
16	5′-RNA-2′ → 4′-*p*-DNA-2′	ACGACGUACU*DMDMDM[h])	38	5038.3	5038.2
17	4′-p-DNA-2′ → 5′-RNA-3′	GTAGUACGUCGU[h])	35	3794.4	3794.6
18	4′-p-DNA-2′ → 5′-RNA-3′	GTGTAGUACGUCGU[h])	33	4427.8	4427.5
19	4′-p-DNA-2′ → 5′-RNA-3′	GTGTGTAGUACGUCGU[h])	30	5061.2	5061.5
20	4′-*p*-DNA-2′	DMDMDM[i])			
21	4′-*p*-DNA-2′	GTGTGT[i])			
22	5′-RNA-3′	GGCGUGUAGGAUAUGCUU CGGCAGAAGGACACGCC[g])	41	11337.9	11340.1
23	4′-p-DNA-2′ → 5′-RNA-2′ → 4′-*p*-DNA-2′	GTGTGTUGUAGGAUAUGC*GGGGG[h])	39	7382.6	7382.1
24	4′-*p*-DNA-2′ → 5′-RNA-2′ → 4′-*p*-DNA-2′	MMMMMGCAGAAGGACA*DMDMDM[h])	44	6985.7	6985
25	5′-RNA-3′	GGCGACCCUGAUGAGGCC GAAAGGCCGAAACCGU[k])			
26	5′-RNA-3′	ACGGUCGGUCGCC[k])			
27	4′-*p*-DNA-2′ → 5′-RNA-3′	MMDDGGTTGCCGAAACCGU[h])	40	6017.9	6018.5
28	5′-RNA-2′ → 4′-*p*-DNA-2′	GGCGACCCUGAUGAGGC*DDMMTTGG[h])	35	8010.1	8008.7

[a]) *p*-DNA part underlined. [b]) U*, C*, and A* from a 3′-*O*-tom-protected phosphoramidite **9**–**12** (*Scheme 1*). [c]) Yield after purification by anion-exchange chromatography; according to capillary electrophoresis, the purity was >98%. [d]) MALDI-TOF-MS: measured in 2,4-dihydroxyacetophenone (ammonium citrate) according to [15]. [e]) a.u. = absorption unit. [f]) For fragment $[M-H]^-$. [g]) Synthesized according to [14]. [h]) Synthesis: see *Exper. Part.* [i]) Synthesis described in [12]. [k]) Synthesis described in [13].

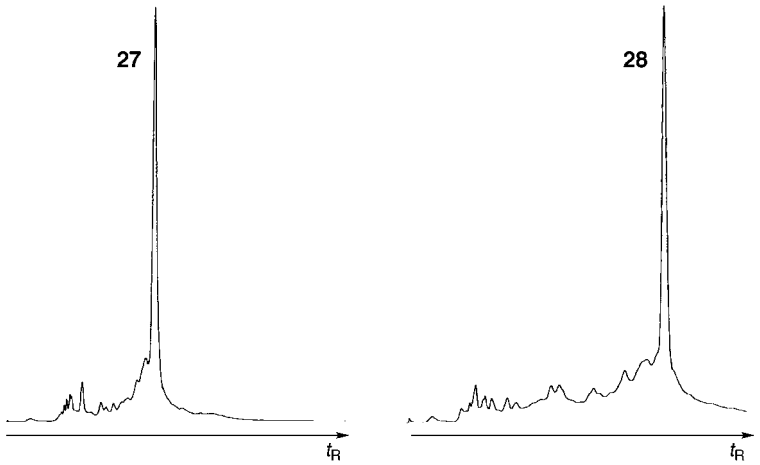

Fig. 3. *Anion-exchange HPLC traces from the crude* p-*DNA/RNA hybrid sequences* **27** *and* **28**, *obtained under preparative conditions* (*SAX* column, 20% *B* → 50% *B* in 30 min, measured at 260 nm; see *Exper. Part*).

They reflect good coupling yields and complete removal of all protecting groups without concomitant strand cleavage.

The crude oligonucleotides sequences **13**–**28** were purified by anion-exchange HPLC and analyzed by MALDI-TOF-MS (*Table 1*). According to capillary gel electrophoresis, their purity was >98%.

2.2. *Pairing Properties of* p-*DNA/RNA Hybrids.* The backbone conformations of the two oligonucleotide pairing systems RNA and *p*-DNA differ substantially from each other. RNA Duplexes adopt the well-known left-handed helical conformation of the *A*-type [16], whereas *p*-DNA duplexes are expected to have an almost linear backbone geometry[4]). In both systems, duplex formation is the result of interstrand H-bonding between complementary nucleobases, and of inter- and intrastrand π-π-stacking interactions between adjacent nucleobases. In order to create stable and rigid *p*-DNA/RNA hybrid structures, we ideally wanted to connect the two, geometrically completely different oligonucleotide pairing systems without interrupting the duplex-stabilizing π-π-stacking interactions at the interface.

Initial model-building studies showed that such an uninterrupted π-π-stacking interaction could occur in hybrid duplexes with 5′-RNA-2′ → 4′-*p*-DNA-2′ and 5′-RNA-3′ → 4′-*p*-DNA-2′ phosphodiester linkages (*Fig. 4*). To test this hypothesis, we compared the stabilities of duplexes formed from both of the two *p*-DNA/RNA hybrid oligonucleotides **15** and **16** (RNA-3′ → 4′-*p*-DNA *vs.* RNA-2′ → 4′-*p*-DNA linkage), and a series of complementary *p*-DNA-2′ → 5′-RNA-linked hybrid sequences with an identical RNA part (complementary to the RNA sequence of **15** and **16**) and a variable *p*-DNA part, designed to form 0, 2, 4, and 6 *p*-DNA base pairs (*Fig. 5*). Each of the RNA/*p*-DNA hybrid sequences **15** and **16** (containing a different RNA → *p*-DNA-linkage) was mixed in a 1:1 ratio with the complementary sequences **14**, **17**, **18**, or **19**,

---

[4]) In analogy to the geometry of *p*-RNA duplexes, determined by NMR spectroscopy [11]. A similar NMR study was carried out with a *p*-DNA duplex, but its structure has not yet been completely determined [17].

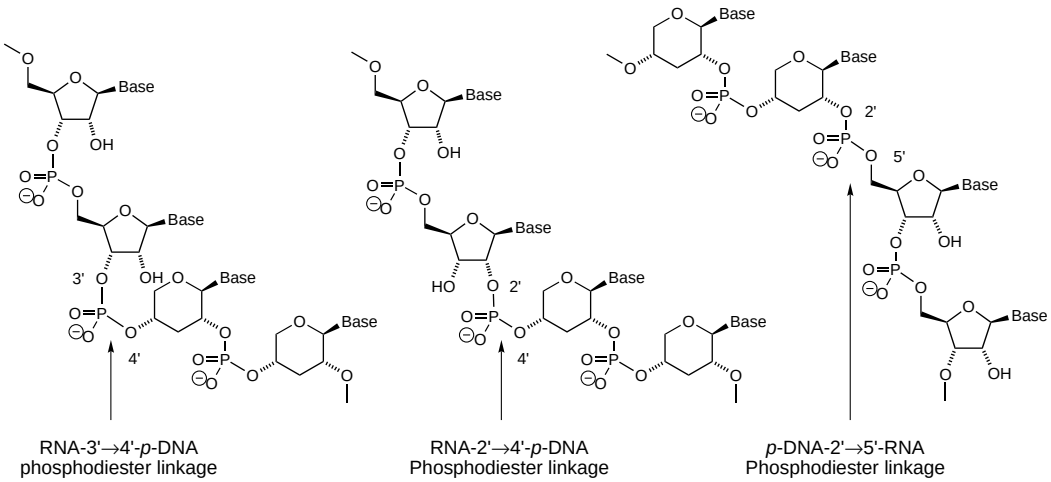

Fig. 4. *Phosphodiester linkages between RNA and* p-*DNA sequences.* Two different linkages (RNA-3′ → 4′-*p*-DNA and RNA-2′ → 4′-*p*-DNA) were investigated as connections between the RNA sequences and the 4′-end of *p*-DNA sequences; the 2′-end of *p*-DNA sequences were always connected to the 5′-end of RNA sequences (*p*-DNA-2′ → 5′-RNA linkages).

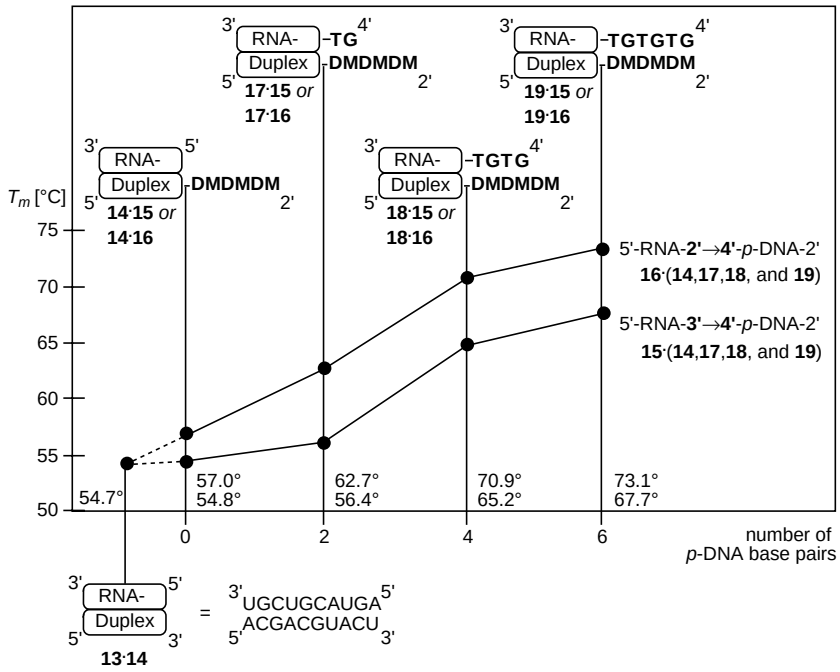

Fig. 5. *Comparison of the pairing properties of* p-*DNA/RNA hybrid duplexes with RNA-3′ → 4′-*p*-DNA or RNA-2′ → 4′-*p*-DNA phosphodiester linkages.* Shown is a graphical representation of the T_m-value dependence from the number of possible *p*-DNA base pairs within a series of *p*-DNA/RNA duplexes. All measurements were carried out at an oligonucleotide single-strand concentration of 10 μM, in 0.15M NaCl at a pH value of 7.0 (0.01M *Tris* · HCl buffer).

and the stabilities of the resulting duplexes were determined by temperature-dependant UV spectroscopy. Only one transition could be detected with all investigated duplexes, and the T_m values were always higher than the T_m values of the corresponding RNA duplex **13**·**14** (T_m 54.7°), or the corresponding *p*-DNA duplex **20**·**21** (T_m 35° [12]), indicating a cooperative interaction between the RNA and the *p*-DNA parts of the hybrid duplexes. However, the type of the phosphodiester linkage between the RNA and the 4′-end of the *p*-DNA part had a significant influence on duplex stability (*Fig. 5*).

The duplex formed from RNA sequence **14** and the RNA-3′ → 4′-*p*-DNA-linked hybrid sequence **15** (→ duplex **14**·**15**) had the same stability as the RNA duplex **13**·**14** ($\Delta T_m = +0.1°$, no *p*-DNA base pairs). Two additional *p*-DNA base pairs (→ duplex **17**·**15**) resulted in a slight increase of duplex stability ($\Delta T_m = +1.6°$, 2 *p*-DNA base pairs), whereas the addition of the next two *p*-DNA base pairs (→ duplex **18**·**15**) increased the stability of the duplex significantly ($\Delta T_m = +8.8°$, 4 *p*-DNA base pairs); addition of the last two base pairs (→ duplex **19**·**15**) resulted in a further duplex stabilization ($\Delta T_m = 2.5°$, 6 *p*-DNA base pairs).

The identical series of experiments was carried out with the hybrid sequence **16**, which differed from **15** by containing a RNA-2′ → 4′-*p*-DNA linkage. The duplex **14**·**16** was more stable than the RNA duplex **13**·**14** ($\Delta T_m = +2.3°$, no *p*-DNA base pairs). Formation of additional *p*-DNA base pairs led to a continuous increase in the stability of the resulting duplexes, with $\Delta T_m = +5.7°$ (duplex **17**·**16**, 2 *p*-DNA base pairs), $\Delta T_m = +8.2°$ (duplex **18**·**16**, 4 *p*-DNA base pairs), and $\Delta T_m = 2.2°$ (duplex **19**·**16**, 6 *p*-DNA base pairs) (*Fig. 5*).

This experiment demonstrated that the two different pairing systems RNA and *p*-DNA can be connected to cooperatively pairing hybrid duplexes, without interrupting π-π-stacking at the interface. When the connection is formed by a RNA-2′ → 4′-*p*-DNA phosphodiester linkage, an immediate increase of duplex stability is achieved, even without the formation of additional *p*-DNA base pairs, such as in duplex **14**·**16**. This so-called 'dangling-end effect' [16] is well-known and is attributed to a favorable stacking interaction between the last base pair and the adjacent, unpaired nucleotide. The immediate and then steadily increasing duplex stabilization observed upon formation of more and more *p*-DNA base pairs demonstrates that the two oligonucleotide systems are not separated, but connected to each other, thereby forming one single continuous pairing system. In contrast, when the connection is formed by a RNA-3′ → 4′-*p*-DNA phosphodiester linkage, cooperative pairing between the two systems is achieved only after formation of 4 base pairs. This indicates that the two base pairs at the *p*-DNA/RNA interface are not stacking with each other and that the two pairing systems are separated.

2.3. *Studies with an Analogue of the FMN-Binding Aptamer*. The flavin mononucleotide (= FMN) binding aptamer **22** (secondary structure: *Fig. 1*) was selected and investigated by *Burgstaller* and *Famulok* [9], and its structure was determined NMR-spectroscopically by *Patel* and co-workers [18]. Two H-bonds between H−N(3) of FMN and N(7) of nucleotide A26 of the aptamer, and O−C(2) of the FMN and HN−C(6) of nucleotide A26 of the aptamer, respectively, together with π-π-stacking interactions result in a quite strong interaction with a K_d value of *ca.* $5 \cdot 10^{-7}$ M [9] (see below, *Fig. 7*). The nucleotide residues responsible for binding the substrate are located

in the central-bulge region of the aptamer; the flanking stem and stem-loop motifs are not interacting with the substrate, but rather responsible for bringing the unpaired nucleotides of the bulge region together [18].

We now prepared two *p*-DNA/RNA hybrid oligonucleotides **23** and **24**, consisting of a central RNA part (identical with the bulge region of the FMN-binding aptamer **22**), and flanked by complementary *p*-DNA sequences (**23**: 4′-*p*d$^{3'}$(GT)$_3$-(RNA sequence)-*p*d$^{3'}$(G)$_5$ – 2′: **24**: 4′-*p*d$^{3'}$(M)$_5$-(RNA sequence)-*p*d$^{3'}$(DM)$_3$-2′). A 1:1 mixture of the oligonucleotides **23** and **24** showed a broad and unsymmetrical transition curve (*Fig. 6*) with a main transition at a temperature of *ca.* 65°. A more continuous, broad transition curve showing no clear transition point was obtained with the aptamer **22**.

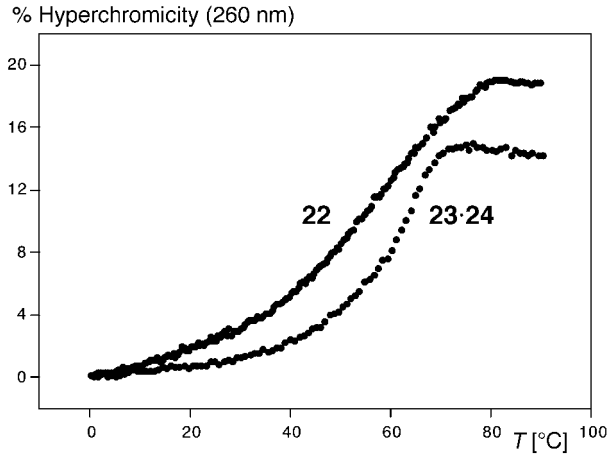

Fig. 6. *Transition curves of the aptamer* **22** *and the analogue* **23**·**24**, *formed from two* p-*DNA/RNA hybrid single strands.* The measurements were carried out at an oligonucleotide single-strand concentration of 10 μM, in 0.15M NaCl/2 mM $MgCl_2$ solution at a pH value of 7.0 (0.01M *Tris*·HCl buffer).

By column retention analysis, *Burgstaller* and *Famulok* have determined a K_d value of $5 \cdot 10^{-7}$ M for the binding of FMN to the aptamer **22** [9]. Since binding of FMN by the aptamer results in efficient quenching of the FMN fluorescence, we performed our binding studies by fluorescence spectroscopy (*Fig. 7*). To 1 μM FMN solutions in 0.15M NaCl and 0.01M *Tris*·HCl buffer (pH 7.4), different amounts of the aptamer **22** or of 1:1 mixtures of the RNA/*p*-DNA hybrid **23**·**24** were added, and the remaining fluorescence intensity at 535 nm was recorded. From these measurements, the dissociation constants K_d could be determined by curve fitting (*Fig. 7*). We found K_d values of $4.6(\pm 0.4) \cdot 10^{-7}$ M and $2.6(\pm 0.3) \cdot 10^{-7}$ M for the binding of FMN to the aptamer **22** and to the RNA/*p*-DNA hybrid **23**·**24**, respectively.

2.4. *Studies with an Analogue of the Hammerhead Ribozyme.* The hammerhead-ribozyme motif, which was discovered in small plant pathogenic RNAs, is a self-cleaving structure that processes multimeric transcripts into monomers during rolling-circle replication of viroid and virusoid RNA genomes [19]. The catalytic motif consists of a small central core surrounded by three helical stems. This structural motif was engineered into a true catalyst by connecting both ends of one stem, thereby forming a

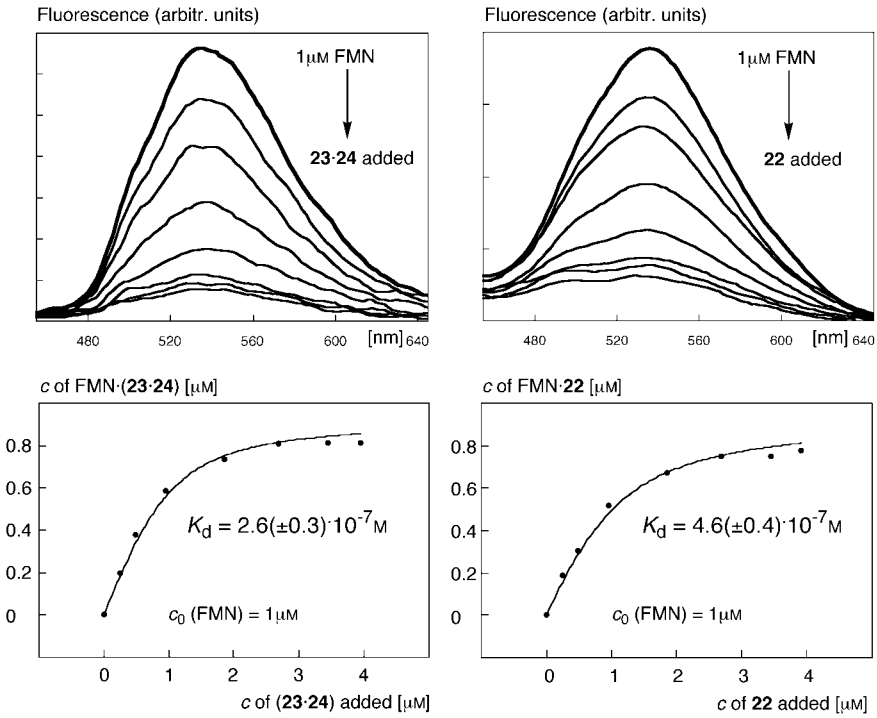

Fig. 7. *Determination of the dissociation constant for binding of FMN to the aptamer* **22** (right) *and the aptamer analogue* **23**·**24** (left) *by fluorescence spectroscopy.* The quenching of the FMN fluorescence upon binding to increasing amounts of added aptamers **22** or **23**·**24** (*top*) was employed to determine individual K_d values (*bottom*). The measurements were carried out in 4 mM $MgCl_2$, 150 mM NaCl, and 10 mM *Tris*·HCl (pH 7.4) at 25°; the excitation wavelength was 420 nm.

hairpin loop (secondary structure: *Fig. 1*, *Scheme 2*); the other two stems are formed *in situ* upon base pairing of the ribozyme sequence and the RNA substrate (*Scheme 2*). In the presence of certain divalent metal ions, such as Mg^{2+} or Mn^{2+}, the ribozyme catalyzes nucleophilic attack of the 2′-OH of one particular (not base pairing) nucleotide of the substrate on its phosphate group; the following transesterification reaction leads finally to strand scission within the RNA substrate [20]. Crystal structures of two different hammerhead-ribozyme constructs were presented by *McKay* and co-workers [8] and by *Scott et al.* [20][21], both revealing its unique wishbone-shaped overall structure and the arrangement of the conserved core nucleotides, which form a large number of noncanonical base pairs.

The *p*-DNA/RNA hybrids **27** and **28** are derived from the hammerhead ribozyme **25** [8] by formal displacement of its stem-loop motif with a complementary *p*-DNA duplex (*Scheme 2*). With this hammerhead analogue **27**·**28**, we carried out cleavage reactions with the RNA substrate **26** under a variety of conditions. As a control, identical reactions were carried out with the ribozyme **25**. Periodically, aliquots were removed and analyzed by anion-exchange HPLC under denaturating conditions. From the time-dependant ratios between the RNA substrate **26** and the sum of the two cleavage

Scheme 2. *Secondary Structure of the Hammerhead Ribozyme* **25** *and the Analogue* **27**·**28** *Formed upon* p-*DNA Base Pairing of the* p-*DNA/RNA Hybrids* **27** *and* **28** (for clarity, the *p*-DNA nucleotides are underlined). After binding of the substrate **26** to the ribozyme **25** or its analogue **27**·**28**, a selective cleavage of a phosphodiester bond occurs (indicated by the arrows).

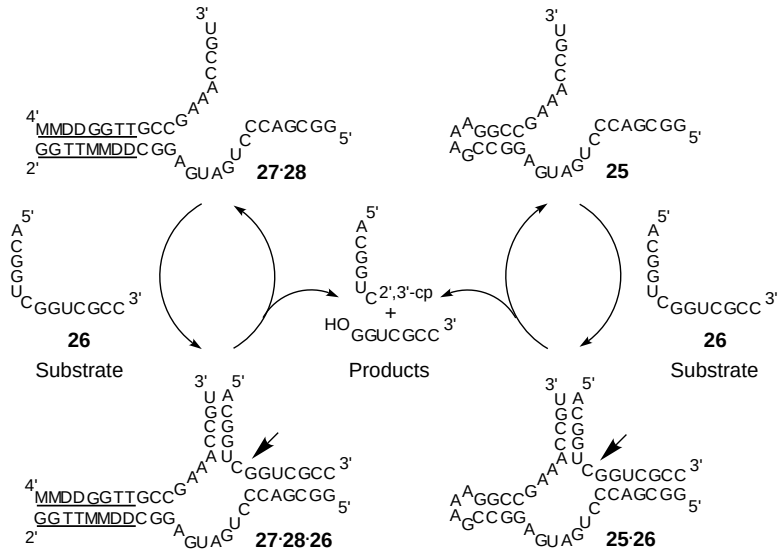

products, pseudo-first-order rate constants were obtained (*Table 2*). As an example, the course of two cleavage reactions, catalyzed by our hammerhead analogue **27**·**28** and the ribozyme **25**, respectively, are illustrated in *Fig. 8* by HPLC traces obtained after different reaction times. The reactions were carried out at a ribozyme concentration of 1 μM, with a 20:1 substrate/ribozyme ratio, in 2 mM $MgCl_2$, 150 mM NaCl, and 10 mM *Tris*·HCl (pH 7.5) at 25°.

Under all reaction conditions, varying the metal ion (Mg^{2+} of Mn^{2+}) and the temperature, our ribozyme analogue **27**·**28** was less active than the parent ribozyme **25**. In *Table 2* and *Fig. 9*, the temperature dependance of the reaction rates in the presence

Table 2. *Pseudo-First-Order Rate Constants for the Cleavage of the Substrate* **26** *by the Ribozyme* **25** *or the Analogue* **27**·**28**, *Determined by HPLC at Different Temperatures and in the Presence of 2 mM* $MgCl_2$ *or 2 mM* $MnCl_2$. Conditions: 1 μM ribozyme or analogue, 20 μM substrate **26**, 150 mM NaCl, and 10 mM *Tris*·HCl (pH 7.5).

2 mM $MgCl_2$			2 mM $MnCl_2$		
T [°C]	k [h^{-1}]		T [°C]	k [h^{-1}]	
	27·**28**	**25**		**27**·**28**	**25**
26	0.005	0.012	26	0.023	0.054
37	0.045	0.057	30	0.052	0.21
42	0.150	0.220	37	0.154	0.61
45	0.170	0.310	42	0.835	1.59
47	0.156	0.358	47	3.40	4.87
			52	2.49	5.70

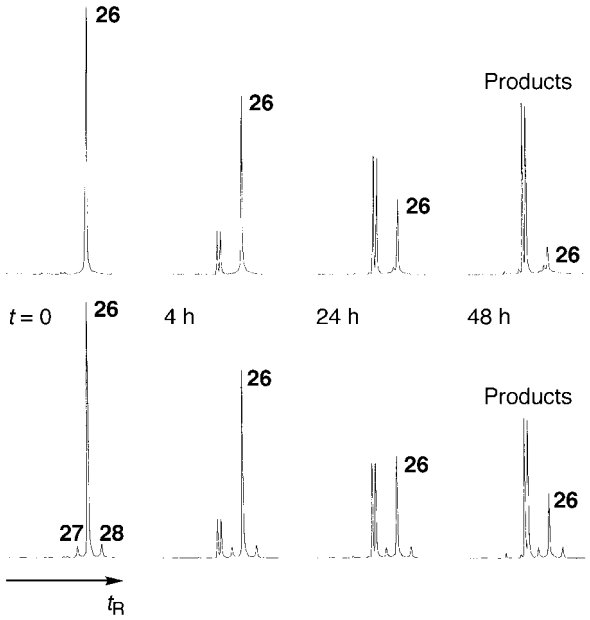

Fig. 8. *Time-course of ribozyme-mediated cleavage reactions of substrate* **26** *with the hammerhead ribozyme* **25** (top) *and the analogue* **27**·**28** (bottom). Shown are anion-exchange HPLC traces obtained under denaturating conditions (20% *B* → 50% *B* in 20 min; measured at 260 nm; see *Exper. Part*). Under these conditions, the two *p*-DNA/RNA sequences **27** and **28** are separated and eluted as single strands (visible as small peaks centered around the substrate peak); the ribozyme **25** is eluted much later and is not shown. The reactions were carried out with 1 μM ribozyme **25** or ribozyme analogue **27**·**28** and 20 μM substrate **26**, in 2 mM $MgCl_2$, 150 mM NaCl, and 10 mM *Tris*·HCl buffer (pH 7.5).

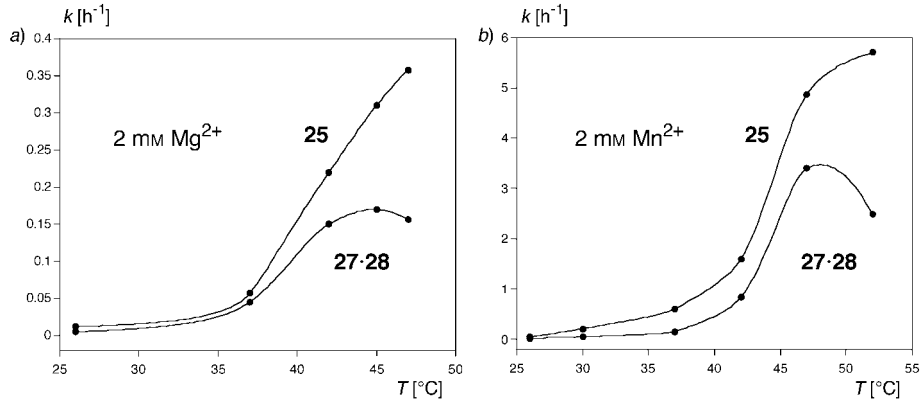

Fig. 9. *Temperature dependance of ribozyme-mediated cleavage reactions of substrate* **26** *with the hammerhead ribozyme* **25** *and the analogue* **27**·**28** a) *of 2 mM* $MgCl_2$ *and* b) *2 mM* $MnCl_2$. For reaction conditions, see *Table 2*.

of 2 mM $MgCl_2$ and 2 mM $MnCl_2$, respectively, is shown. With 2 mM $MgCl_2$ and in the temperature range of 26–42°, the ribozyme **25** was *ca.* 1.5 times more efficient than the analogue **27**·**28** (*Table 2*). The catalytic activity of the ribozyme **25** increased steadily

between 37° and 47°, whereas the activity of the ribozyme analogue **27**·**28** reached an optimum at 45°. A qualitatively similar result was obtained by performing the same experiments with Mn^{2+}. Both, the ribozyme **25** and the analogue **27**·**28** were significantly more active in the presence of 2 mM $MnCl_2$ than in the presence of 2 mM $MgCl_2$. Upon increasing the reaction temperature, the relative differences in catalytic efficiency of ribozyme **25** and analogue **27**·**28** decreased steadily from a factor of *ca.* 4 at 30° to a factor of *ca.* 1.4 at 47°. The analogue **27**·**28** showed again an optimum activity around 50°.

The occurrence of a temperature optimum for the catalytic activity of the ribozyme analogue **27**·**28** agrees very well with its strand dissociation between 40° and 70°, determined by temperature-dependent UV spectroscopy (*Fig. 10*).

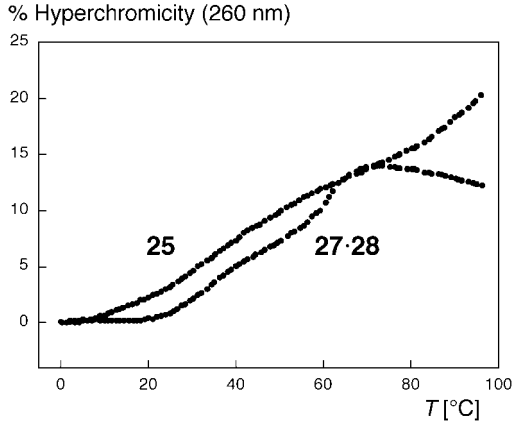

Fig. 10. *Transition curves of the ribozyme* **25** *and the analogue* **27**·**28**, *formed from two* p-*DNA/RNA hybrid single strands.* The measurements were carried out at an oligonucleotide single-strand concentration of 10 μM, in 0.15M NaCl/2 mM $MgCl_2$ at a pH value of 7.5 (0.01M *Tris*·HCl buffer).

3. Discussion. – This model study demonstrates that complementary *p*-DNA duplexes formed from *p*-DNA/RNA hybrid sequences are efficient substitutes of RNA stem/loop and stem structures. The two functional aptamer and ribozyme analogues, prepared and investigated in this study, were formed in solution by base pairing of two short, complementary *p*-DNA sequences, each connected to a central RNA sequence. The *p*-DNA part served thereby as structural/architectural element, whereas the RNA part was responsible for their function.

The formation of (potentially) functional oligonucleotides from several single strands allows the creation and evaluation of a great number of different structures from a small number of different single strands, by simply mixing them. A number of 100 different oligonucleotide complexes could be prepared, for example, from two sets of such complementary single strands, each set consisting of only 10 different sequences. Furthermore, these relatively short sequences are easy to synthesize and to purify. By employing *p*-DNA sequences as structural elements instead of complementary RNA or DNA sequences, a minimal interaction between them and the functional part, consisting of RNA nucleotides, can be expected.

We are now about to synthesize and to evaluate a number of aptamer and ribozyme analogues consisting of two *p*-DNA/RNA hybrid single strands and containing different modified RNA nucleotides.

This work was supported by the *Swiss National Science Foundation* (Project Nr. 20-61741.00). We thank Prof. *Andrea Vasella*, ETH Zürich, for giving us generous access to his fluorescence spectrometer.

Experimental Part

General. See [12]. Additionally: HPLC: *Nucleogel SAX 1000-8/46* (*Macherey & Nagel*, Nr. 719469), flow 0.5 ml/min, $A \rightarrow B$ in 45 min (*A:* 20 mM sodium phosphate in H_2O, pH 11.5; *B:* 20 mM sodium phosphate/2M NaCl in H_2O, pH 11.5), detection at 260 nm, elution at 25°. Fluorescence spectroscopy: *ISS-K2* multifrequency phase fluorometer.

Oligonucleotide Synthesis and Deprotection. The RNA oligonucleotides **13**, **14**, **22**, **25**, and **26** were prepared from 2′-*O*-tom-protected ribonucleoside phosphoramidites **5**–**8** according to [14]; the *p*-DNA/RNA hybrid oligonucleotides **15**–**19**, **23**, **24**, **27**, and **28** were assembled on a *Pharmacia Gene Assembler Plus* from phosphoramidites **1**–**12** by the conditions described in [12] (2.5 min coupling time for RNA phosphoramidites **5**–**12** and 5 min coupling time tor *p*-DNA phosphoramidites **1**–**4**). All syntheses were carried out on a 1-μmol scale and in the 'trityl-off' mode. After the assembly, the solid supports were removed from the cartridges and treated with a 1:1 mixture of 12M $MeNH_2$ in H_2O and 8M $MeNH_2$ in EtOH (1.5 ml) for 3 h at 25°. By centrifugation, the supernatant solns. were separated from the solid supports and evaporated and the residues dissolved in 1M $Bu_4NF \cdot 3\,H_2O$ in THF/1-methylpyrrolidin-2-one 1:1 (1 ml) for 14 h at 25°. The reactions were quenched by addition of 1M *Tris* · HCl buffer (pH 7.4, 1 ml), and the products were desalted by chromatography on a *Sephadex G-10* column (1.5 × 25 cm, elution with H_2O, 1 ml/min).

Thermal Denaturation Measurements. Absorbance *vs.* temp. profiles were recorded in fused-quartz cuvettes at 260 nm on a *Cary Bio-1* spectrophotometer equipped with a *Peltier* temp.-controlling device. The samples were prepared from stock solns. of the oligonucleotide (or 1:1 mixtures of oligonucleotides), 1M *Tris* · HCl buffer (pH 7.0), 3M NaCl, and 50 mM $MgCl_2$ and subsequently degassed. A layer of silicon oil was placed on the surface of the soln. Prior to the measurements, each sample was briefly heated to 80°.

FMN-Binding Assay. To 1.5 ml of an aq. soln. containing FMN (1 μM), $MgCl_2$ (4 mM), NaCl (150 mM), and *Tris* · HCl (10 mM, pH 7.4) were added stepwise aliquots of aq. solns. containing **22** (25 μM) or **23** + **24** (25 + 25 μM, resp.), $MgCl_2$ (4 mM), NaCl (150 mM), and *Tris* · HCl (10 mM, pH 7.4). After addition of each aliquot, the fluorescence emission spectrum was recorded in the range of 450–650 nm (excitation at 420 nm, see *Fig. 7*). The dissociation constant K_d of the FMN · aptamer complex is defined as: $K_d = [A][F]/[AF]$, where [A] is the aptamer concentration (**22** or **23** · **24**), [F] the FMN concentration, and [AF] the concentration of the complex. Assuming that the aptamer-bound FMN shows no fluorescence emission, the equilibrium concentration of [AF] was determined from the ratio of remaining fluorescence emission at 535 nm. A plot of [AF] *vs.* $[A_{tot}]$ was then iteratively fitted to the function $2[AF] = [A_{tot}] + [F_{tot}] + K_d - \{([A_{tot}] + [F_{tot}] + K_d)^2 - 4[A_{tot}][F_{tot}]\}^{0.5}$, where $[A_{tot}]$ and $[F_{tot}]$ are the total aptamer and FMN concentrations, resp. The resulting curves and the calculated K_d values for the aptamer **22** and the analogue **23** · **24** are shown in *Fig. 7*.

Ribozyme-Mediated Cleavage Reactions. Separately, three aqueous buffer solns. containing NaCl (150 mM), *Tris* · HCl buffer (10 mM, pH 7.5), and either the substrate **26** (100 μM), the ribozyme **25** (1.4 μM), or the analogue **27** · **28** (1.4 μM + 1.4 μM) were heated to 90° for 1 min and then cooled to 25°. To 180 μl of each of these three solns. 20 μl of an aq. soln. containing NaCl (150 mM), *Tris* · HCl buffer (10 mM, pH 7.5), and either $MgCl_2$ (20 mM) or $MnCl_2$ (20 mM) was added. The solns. were incubated for 10 min at the reaction temp. (see *Table 2*), and then the reactions were initialized by adding 50 μl of the soln. containing the substrate **26** to the solns. containing either the ribozyme **25** or the analogue **27** · **28**. The two reaction mixtures (volume 250 μl) contained 1 μM ribozyme **25** or ribozyme analogue **27** · **28**, 20 μM substrate, 150 mM NaCl, 10 mM *Tris* · HCl buffer (pH 7.5), and 2 mM $MgCl_2$ or $MnCl_2$. At appropriate time intervals, aliquots of 50 μl were withdrawn, quenched with 0.2M aq. NaH_2PO_4 (20 μl; → pH 4.5), and analyzed by anion-exchange HPLC (*SAX* column; 20% $B \rightarrow$ 50% *B* in 20 min). The integral ratios between the signals of the substrate **26** and the sum of the two cleavage products (*Fig. 8*) were then translated into individual pseudo-first-order rate constants (*Table 2*).

5′-O-(4,4′-Dimethoxytrityl)-3′-O-{[(triisopropylsilyl)oxy]methyl}uridine 2′-(2-Cyanoethyl Diisopropylphosphoramidite) (**9**). A soln. of 5′-*O*-(4,4′-dimethoxytrityl)-3′-*O*-{[(triisopropylsilyl)oxy]methyl}uridine [14] (1.46 g, 20 mmol) in CH_2Cl_2 (8 ml) was treated consecutively with $^iPr_2NEt$ (1.06 ml, 50 mmol) and 2-cyanoethyl

diisopropylphosphoramidochloridite (0.56 g, 24 mmol). After stirring for 14 h at 25°, the mixture was subjected to CC (SiO_2 (50 g), hexane/AcOEt 9:1 → 3:7 (+ 3% Et_3N)): **10** (1.7 g, 92%). Colorless foam (1:1 mixture of diastereoisomers). TLC (hexane/AcOEt 1:1): R_f 0.65. UV (MeCN): 264 (12000), 236 (24000), 225 (20000). ^{1}H-NMR (400 MHz, $CDCl_3$): 0.97 – 1.09 (*m*, ^{i}Pr$_3$Si); 1.17, 1.18 (2*d*, *J* = 6.8, (*Me*$_2$CH)$_2$N); 2.58 – 2.69 (*m*, C*H*$_2$CN); 3.40, 3.42 (2*d*, *J* = 4.6, H–C(5′)); 3.56 – 3.66 (*m*, 3 H, (Me$_2$C*H*)$_2$N, POCH$_2$); 3.792, 3.795, 3.797 (3*s*, 2 MeO); 3.76 – 3.94 (*m*, 2 H, H–C(5′), POCH$_2$); 4.27 – 4.32, 4.43 – 4.51 (2*m*, H–C(2′), H–C(3′), H–C(4′)); 4.93 – 5.00 (*m*, OCH$_2$O); 5.26, 5.28 (2*d*, *J* = 8.1, H–C(5)); 6.08 (*d*, *J* = 3.8, 0.5 H, H–C(1′)); 6.11 (*d*, *J* = 3.3, 0.5 H, H–C(1′)); 6.81 – 6.85 (*m*, 4 arom. H); 7.22 – 7.40 (*m*, 9 arom. H); 7.97, 7.99 (2*d*, *J* = 8.1, H–C(6)); 8.80 (br. *s*, H–N(3)). ^{13}C-NMR (100 MHz, $CDCl_3$): 11.89, 11.91 (2*d*, (Me$_2$*C*H)$_3$Si); 17.5, 17.8, 17.9 (3*q*, (*Me*$_2$CH)$_3$Si); 20.2, 20.3 (2*t*, *C*H$_2$CN); 24.39, 24.47, 24.50, 24.56, 24.61, 24.68 (6*q*, (*Me*$_2$CH)$_2$N); 43.4, 43.5 (2*d*, *J*(C,P) = 12, (Me$_2$*C*H)$_2$N); 55.2 (*q*, MeO); 58.5, 58.6 (2*t*, *J*(C,P) = 17, POCH$_2$); 61.9, 62.1 (2*t*, C(5′)); 72.5 (*d*, *J*(C,P) = 5), 73.7 (*d*), 75.4, 76.0 (2*d*, *J*(C,P) = 16), 82.2 (*d*, *J*(C,P) = 24), (C(2′), C(3′), C(4′)); 87.1, 87.2 (2*s*, arom. C); 88.0 (*d*, *J*(C,P) = 5, C(1′)); 88.3 (*d*, C(1′)); 88.9, 89.4 (2*t*, OCH$_2$O); 102.1 (*d*, C(5)); 113.24, 113.26 (2*d*, arom. C); 117.5, 117.9 (2*s*, CN); 127.16, 127.20, 127.9, 128.0, 128.2, 130.2, 130.3 (7*d*, arom. C); 135.03, 135.07, 135.13, 135.20 (4*s*, arom. C); 140.2, 140.3 (2*d*, C(6)); 144.2, 144.3 (2*s*, arom. C); 150.0, 150.3 (2*s*, C(2)); 158.69, 158.72, 158.75 (3*s*, arom. C); 163.0, 163.1 (2*s*, C(4)). ^{31}P-NMR (150 MHz, $CDCl_3$): 150.9; 151.3. HR-MALDI-MS: 955.442 ([*M* + Na]$^+$, $C_{51}H_{72}N_5NaO_{10}PSi^+$; calc. 955.442).

N^4-*Acetyl-5′-*O*-(4,4′-dimethoxytrityl)-3′-*O*-{[(triisopropyl)silyloxy]methyl}cytidine 2′-(2-Cyanoethyl Diisopropylphosphoramidite)* (**10**). As described for **9**, with *N*^{4}-acetyl-5′-*O*-(4,4′-dimethoxytrityl)-3′-*O*-{[(triisopropyl)silyloxy]methyl}cytidine [14] (1.6 g, 20 mmol), CH_2Cl_2 (8 ml), ^{i}Pr$_2$NEt (1.06 ml, 50 mmol), and 2-cyanoethyl diisopropylphosphoramidochloridite (0.56 g, 24 mmol). CC (SiO_2 (50 g), hexane/AcOEt 9:1 → 3:7 (+ 3% Et_3N)): **10** (1.75 g, 90%). Colorless foam (1:1 mixture of diastereoisomers). TLC (hexane/AcOEt 3:7): R_f 0.75. ^{1}H-NMR (400 MHz, $CDCl_3$): 0.98 – 1.10 (*m*, ^{i}Pr$_3$SiO); 1.16, 1.17, 1.18, 1.20 (4*d*, *J* = 6.8, (*Me*$_2$CH)$_2$N); 2.22 (*s*, MeCO); 2.63, 2.70, 2.77, 2.81 (4*t*, *J* = 6.5, C*H*$_2$CN); 3.38 – 3.46, 3.60 – 3.75 (2*m*, 4 H, POCH$_2$, (Me$_2$C*H*)$_2$N, H–C(5′)); 3.811, 3.813, 3.815 (3*s*, 2 MeO); 3.84 – 4.08 (*m*, 2 H, H–C(5′), POCH$_2$); 4.31 – 4.36, 4.45 – 4.54 (2*m*, H–C(2′), H–C(3′), H–C(4′)); 4.86 – 4.93 (*m*, OCH$_2$O); 6.04 (*s*, 0.5 H, H–C(1′)); 6.10 (*d*, *J* = 1.3, 0.5 H, H–C(1′)); 6.83 – 6.86 (*m*, 4 arom. H); 6.96, 6.99 (2*d*, *J* = 7.4, H–C(5)); 7.25 – 7.42 (*m*, 9 arom. H); 8.50 (*t*, *J* = 7.6, H–C(6)); 9.23, 9.34 (2 br. *s*, NH–C(4)). ^{13}C-NMR (100 MHz, $CDCl_3$): 11.88, 11.91 (2*d*, (Me$_2$*C*H)$_3$Si); 17.80, 17.83, 17.85 (3*q*, (*Me*$_2$CH)$_3$Si); 20.2, 20.3 (2*t*, *J*(C,P) = 7, *C*H$_2$CN); 24.38, 24.46, 24.48, 24.54, 24.57, 24.68, 24.75, 24.93 (8*q*, (*Me*$_2$CH)$_2$N, *Me*CO); 43.4, 43.5, 43.6 (3*d*, (Me$_2$*C*H)$_2$N); 55.2 (*q*, MeO); 58.5, 58.9 (2*t*, *J*(C,P) = 20, POCH$_2$); 61.3 (*t*, C(5′)); 70.9, 71.5 (2*d*), 74.8 (*d*, *J*(C,P) = 14), 76.1 (*d*, *J*(C,P) = 20), 81.2 (*d*, *J*(C,P) = 4) (C(2′), C(3′), C(4′)); 87.1 (*s*, arom. C); 88.4, 88.8 (2*d*, C(1′)); 90.3, 90.4, 90.5 (3*t*, OCH$_2$O); 96.3 (*d*, C(5)); 113.3 (*d*, arom. C); 117.7, 118.2 (2*s*, CN); 127.2, 128.0, 128.4, 130.3 (4*d*, arom. C); 135.17, 135.19, 135.27, 135.32, 144.13, 144.16 (6*s*, arom. C); 144.9, 145.1 (2*d*, C(6)); 154.8, 155.0 (2*s*, C(2)); 158.70, 158.72 (2*s*, arom. C); 162.5, 162.6 (2*s*, C(4)); 170.2 (*s*, CO). ^{31}P-NMR (150 MHz, $CDCl_3$): 150.6; 150.9. HR-MALDI-MS: 996.468 ([*M* + Na]$^+$, $C_{51}H_{72}N_5NaO_{10}PSi^+$; calc. 996.486).

N^2-*Acetyl-5′-*O*-(4,4′-dimethoxytrityl)-3′-*O*-{[(triisopropylsilyl)oxy]methyl}guanosine 2′-(2-Cyanoethyl Diisopropylphosphoramidite)* (**11**). As described for **9**, with *N*^{2}-acetyl-5′-*O*-(4,4′-dimethoxytrityl)-3′-*O*-{[(triisopropylsilyl)oxy]methyl}guanosine [14] (1.6 g, 20 mmol), CH_2Cl_2 (8 ml), ^{i}Pr$_2$NEt (1.06 ml, 50 mmol), and 2-cyanoethyl diisopropylphosphoramidochloridite (0.56 g, 24 mmol). CC (SiO_2 (50 g), hexane/AcOEt 1:1 → AcOEt, then AcOEt → AcOEt/MeOH 9:1 (+ 3% Et_3N)): **20** (1.7 g, 85%). Colorless foam (1:1 mixture of diastereoisomers). TLC (hexane/AcOEt 3:7): R_f 0.50. ^{1}H-NMR (400 MHz, $CDCl_3$): 0.88 (*d*, *J* = 6.8, 2 H, (*Me*$_2$CH)$_2$N); 0.93 – 1.05 (*m*, ^{i}Pr$_3$SiO); 1.08 – 1.17 (3*d*, *J* = 6.8, 10 H, (*Me*$_2$CH)$_2$N); 1.69 (*s*, MeCO); 2.48, 2.62, 2.71 (3*t*, *J* = 6.1, CH$_2$CN); 3.26, 3.32 (2*dd*, *J* = 4.1, 10.7, H–C(5′)); 3.46 – 3.62 (*m*, 4 H, (Me$_2$C*H*)$_2$N, H–C(5′), POCH$_2$); 3.763, 3.767, 3.772, 3.776 (4*s*, 2 MeO); 3.90 (*t*, *J* = 6.4, 1 H, POCH$_2$); 4.33 – 4.46 (*m*, H–C(2′), H–C(4′)); 4.91, 4.97, 5.03, 5.09 (4*d*, *J* = 5.2, OCH$_2$O); 5.21 – 5.30 (*m*, H–C(3′)); 5.92 (*d*, *J* = 7.4, 0.5 H, H–C(1′)); 5.95 (*d*, *J* = 7.4, 0.5 H, H–C(1′)); 6.76 – 6.82 (*m*, 4 arom. C); 7.14 – 7.53 (*m*, 9 arom. H); 7.79 (*s*, H–C(8)); 8.30 (br. *s*, NH–C(2)); 11.7 (br. *s*, H–N(1)). ^{13}C-NMR (100 MHz, $CDCl_3$): 11.82, 11.86 (2*d*, (Me$_2$*C*H)$_3$Si); 17.79, 17.82 (2*q*, (*Me*$_2$CH)$_3$Si); 20.1 (*t*, *J*(C,P) = 7, *C*H$_2$CN); 20.3 (*t*, *J*(C,P) = 6, *C*H$_2$CN); 23.47, 23.54 (2*q*, *Me*CO); 24.2, 24.3, 24.51, 24.53, 24.57, 24.62 (6*q*, (*Me*$_2$CH)$_2$N); 43.1 (*d*, (Me$_2$*C*H)$_2$N); 43.3 (*d*, *J*(C,P) = 12, (Me$_2$*C*H)$_2$N); 55.2 (*q*, MeO); 57.7, 58.1 (2*t*, *J*(C,P) = 17, POCH$_2$); 63.5, 63.8 (2*t*, C(5′)); 74.2 (*d*, *J*(C,P) = 15), 74.9 (*d*, *J*(C,P) = 16), 75.1 (*d*, *J*(C,P) = 4), 77.2 (*d*), 83.2 (*d*), 84.6 (*d*) (C(2′), C(3′), C(4′)); 86.38 (*s*, arom. C); 87.8, 88.9 (2*d*, *J*(C,P) = 9, C(1′)); 89.7, 90.2 (2*t*, OCH$_2$O); 113.16, 113.20, 113.22 (3*d*, arom. C); 117.9, 118.1 (2*s*, CN); 122.2, 122.4 (2*s*, C(5)); 127.0, 127.90, 127.97, 128.0, 128.1, 128.3, 130.0 (7*d*, arom. C); 135.60, 135.64, 136.0 (3*s*, arom. C); 138.7, 138.8 (2*d*, C(8)); 144.9, 145.0 (2*s*, arom. C); 146.6, 146.9 (2*s*, C(4)); 148.20,

148.25 (2*s*, C(2)); 155.6 (*s*, C(6)); 158.6 (2*s*, arom. C); 171.5, 171.6 (2*s*, CO). ^{31}P-NMR (150 MHz, $CDCl_3$): 149.9; 150.5. HR-MALDI-MS: 1036.474 ($[M+Na]^+$, $C_{52}H_{72}N_7NaO_{10}PSi^+$; calc. 1036.474).

N^6-*Benzoyl-5′*-O-*(4,4′-dimethoxytrityl)-3′*-O-*{[(triisopropylsilyl)oxy]methyl}adenosine 2′-(2-Cyanoethyl Diisopropylphosphoramidite)* (**12**). As described for **9**, with *N*^{6}-benzoyl-5′-*O*-(4,4′-dimethoxytrityl)-3′-*O*-{[(triisopropylsilyl)oxy]methyl}adenosine [14] (1.6 g, 20 mmol), CH_2Cl_2 (8 ml), ^{i}Pr$_2$NEt (1.06 ml, 50 mmol), and 2-cyanoethyl diisopropylphosphoramidochloridite (0.56 g, 24 mmol). CC (SiO_2 (50 g), hexane/AcOEt 9:1 → 3:7 (+ 3% Et_3N)): **12** (1.9 g, 90%). Colorless foam (1:1 mixture of diastereoisomers). TLC (hexane/AcOEt 3:7): R_f 0.80. ^{1}H-NMR (400 MHz, $CDCl_3$): 0.92–1.09 (*m*, 24 H, ^{i}Pr$_3$SiO, $(Me_2CH)_2N$); 1.11, 1.12, 1.15 (3*d*, *J* = 6.8, 9 H, $(Me_2CH)_2N$); 2.41 (*dt*, *J* = 1.6, 6.4, 1 H, CH_2CN); 2.58 (*t*, *J* = 6.8, 1 H, CH_2CN); 3.38 (*dt*, *J* = 4.4, 10.7, 1 H, $POCH_2$); 3.47–3.75 (*m*, 4 H, $POCH_2$, $(Me_2CH)_2N$, H–C(5′)); 3.772, 3.774 (2*s*, 2 MeO); 3.79–3.90 (*m*, 1 H, $(Me_2CH)_2N$); 4.44, 4.48 (2*q*, *J* = 4.2, H–C(4′)); 4.56, 4.60 (2*t*, *J* = 4.6, H–C(2′)); 4.96, 5.00 (2*d*, *J* = 4.9, 1 H, OCH_2O); 5.05–5.10 (*m*, 1.5 H, H–C(3′), OCH_2O); 5.16 (*q*, *J* = 5.1, 0.5 H, H–C(3′)); 6.22, 6.30 (2*d*, *J* = 5.2, H–C(1′)); 6.78–6.80 (*m*, 4 arom. H); 7.18–7.62 (*m*, 14 arom. H); 8.24, 8.27 (2*s*, H–C(2)); 9.10 (br. *s*, NH–C(6)); 8.71, 8.73 (2*s*, H–C(8)). ^{13}C-NMR (100 MHz, $CDCl_3$): 11.9 (*d*, $(Me_2CH)_3Si$); 17.82, 17.85 (2*q*, $(Me_2CH)_3Si$); 20.0, 20.2 (2*t*, *J*(C,P) = 6, CH_2CN); 24.25, 24.32, 24.48, 24.51, 24.54, 24.58, 24.66 (7*q*, $(Me_2CH)_2N$); 43.2, 43.4 (2*d*, *J*(C,P) = 9, $(Me_2CH)_2N$); 55.2 (1*q*, MeO); 58.1, 58.9 (2*t*, *J*(C,P) = 18, $POCH_2$); 63.2 (*t*, C(5′)); 74.5, 74.7 (2*d*, *J*(C,P) = 17), 75.5, 75.6 (2*d*), 83.1, 83.3 (2*d*) C(2′), C(3′), C(4′)); 86.61, 86.62 (2*s*, arom. C); 87.7, 87.9 (2*d*, C(1′)); 89.4, 89.8 (2*t*, OCH_2O); 113.16, 113.32 (2*d*, arom. C); 117.4, 117.5 (2*s*, CN); 123.26, 123.32 (2*s*, C(5)); 126.9, 127.8, 127.9, 128.20, 128.22, 128.9, 130.1, 132.7 (8*d*, arom. C); 135.64, 135.66, 135.7 (3*s*, arom. C); 141.8, 142.0 (2*d*, C(8)); 144.51, 144.55 (2*s*, arom. C); 149.47, 149.50 (2*s*, C(4)); 151.6, 151.8 (2*s*, C(6)); 152.6, 152.7 (2*d*, C(2)); 158.5 (*s*, arom. C); 164.5, 164.6 (2*s*, CO). ^{31}P-NMR (150 MHz, $CDCl_3$): 150.8; 151.5. HR-MALDI-MS: 1082.495 ($[M+Na]^+$, $C_{57}H_{74}N_7NaO_9PSi^+$; calc. 1082.495).

REFERENCES

[1] T. R. Cech, A. J. Zaug, P. J. Grabowski, *Cell* **1981**, *27*, 487; K. Kruger, P. J. Grabowski, A. Zaug, J. Sands, D. E. Gottschling, T. R. Cech, *Cell* **1982**, *31*, 147; C. Guerruer-Takada, K. Gardiner, T. Marsh, N. Pace, S. Altman, *Cell* **1983**, *35*, 849.

[2] M. Egli, *Angew. Chem., Int. Ed.* **1997**, *36*, 480.

[3] X. Wu, S. Pitsch, *Nucleic Acids Res.* **1998**, *26*, 4315.

[4] X. Wu, S. Pitsch, *Bioconjugate Chem*. **1999**, *10*, 921.

[5] X. Wu, S. Pitsch, *Helv. Chim. Acta* **2000**, *83*, 1127.

[6] S. Klug, M. Famulok, *Mol. Biol. Reports* **1994**, *20*, 97.

[7] D. Xiaochang, G. F. Joyce, *Helv. Chim. Acta* **2000**, *83*, 1701; S. W. Sanatoro, G. F. Joyce, K. Sakthivel, S. Gramatikova, C. F. Barbas, *J. Am. Chem. Soc*. **2000**, *122*, 2433; T. W. Wiegand, R. C. Janssen, B. E. Eaton, *Chem. Biol*. **1997**, *4*, 675; T. M. Tarasow, S. L. Tarasow, B. E. Eaton, *Nature (London)* **1997**, *389*, 54.

[8] H. E. Pley, K. M. Flaherty, D. B. McKay, *Nature (London)* **1994**, *372*, 68.

[9] P. Burgstaller, M. Famulok, *Angew. Chem., Int. Ed.* **1994**, *33*, 1084.

[10] S. Pitsch, S. Wendeborn, B. Jaun, A. Eschenmoser, *Helv. Chim. Acta* **1993**, *76*, 2161; S. Pitsch, R. Krishnamurthy, M. Bolli, S. Wendeborn, A. Holzner, M. Minton, C. Lesueur, I. Schlönvogt, B. Jaun, A. Eschenmoser, *Helv. Chim. Acta* **1995**, *78*, 1621; R. Krishnamurthy, S. Pitsch, M. Minton, C. Miculka, N. Windhab, A. Eschenmoser, *Angew. Chem., Int. Ed.* **1996**, *35*, 1537; M. Bolli, R. Micura, S. Pitsch, A. Eschenmoser, *Helv. Chim. Acta* **1997**, *80*, 1901.

[11] I. Schlönvogt, S. Pitsch, C. Lesueur, A. Eschenmoser, B. Jaun, R. M. Wolf, *Helv. Chim. Acta* **1996**, *79*, 2316.

[12] D. Ackermann, S. Pitsch, *Helv. Chim. Acta* **2002**, *85*, 1443.

[13] S. Pitsch, P. A. Weiss, X. Wu, D. Ackermann, T. Honegger, *Helv. Chim. Acta* **1999**, *82*, 1753.

[14] S. Pitsch, P. A. Weiss, L. Jenny, A. Stutz, X. Wu, *Helv. Chim. Acta* **2001**, *84*, 3773.

[15] U. Pieles, W. Zürcher, H. Moser, *Nucleic Acids Res.* **1993**, *21*, 3191.

[16] W. Saenger, 'Principles of Nucleic Acid Structure', Springer-Verlag, New York-Berlin-Heidelberg-Tokyo, 1983.

[17] M.-O. Ebert, D. Ackermann, S. Pitsch, B. Jaun, *Chimia* **2001**, *55*, 852.

[18] P. Fan, A. K. Suri, R. Fiala, D. Live, D. J. Patel, *J. Mol. Biol*. **1996**, *258*, 480.

[19] T. Forster, R. Symons, *Cell* **1987**, *49*, 211.

[20] W. G. Scott, J. B. Murray, J. R. P. Arnold, B. L. Stoddard, A. Klug, *Science (Washington, D.C.)* **1996**, *271*, 2065; J. B. Murray, D. P. Terwey, L. Maloney, A. Karpeisky, N. Usman, L. Beigelman, W. G. Scott, *Cell* **1998**, *92*, 665.
[21] W. G. Scott, J. T. Finch, A. Klug, *Cell* **1995**, *81*, 991.

Received December 5, 2001